RESEARCH ARTICLE | FEBRUARY 03 2026

Cryogenic amplifier with high sensitivity and stability for noise-STM

Maialen Ortego Larrazabal ; Jiasen Niu ; Jian-Feng Ge ; Yudai Sato ; Jan P. Cuperus ; Tjerk Benschop; Koen M. Bastiaans; Amber Mozes ; Ingmar Swart ; Milan P. Allan

Rev. Sci. Instrum. 97, 023701 (2026)
https://doi.org/10.1063/5.0300260

Review of Scientific Instruments ARTICLE pubs.aip.org/aip/rsi

Cryogenic amplifier with high sensitivity and stability for noise-STM

Cite as: Rev. Sci. Instrum. 97, 023701 (2026); doi: 10.1063/5.0300260
Submitted: 1 September 2025 • Accepted: 24 December 2025 •
Published Online: 3 February 2026

Maialen Ortego Larrazabal,[1,2] Jiasen Niu,[1,3,4,5] Jian-Feng Ge,[1,6] Yudai Sato,[1,3,4,5] Jan P. Cuperus,[2] Tjerk Benschop,[1] Koen M. Bastiaans,[7] Amber Mozes,[1] Ingmar Swart,[2,a)] and Milan P. Allan[1,3,4,5,a)]

AFFILIATIONS

[1] Leiden Institute of Physics, Leiden University, Niels Bohrweg 2, 2333 CA Leiden, The Netherlands
[2] Debye Institute of Nanomaterials Science, Utrecht University, P.O. Box 80000, 3508 TA Utrecht, The Netherlands
[3] Faculty of Physics, Ludwig-Maximilians-University Munich, Munich 80799, Germany
[4] Munich Center for Quantum Science and Technology (MCQST), Ludwig-Maximilians-University Munich, München 80799, Germany
[5] Center for Nano Science (CeNS), Ludwig-Maximilians-University Munich, Munich 80799, Germany
[6] Max Planck Institute for Chemical Physics of Solids, 01187 Dresden, Germany
[7] Kavli Institute of Nanoscience, Delft University of Technology, 2628 CJ Delft, The Netherlands

[a)] **Authors to whom correspondence should be addressed:** i.swart@uu.nl and milan.allan@lmu.de

ABSTRACT

Local shot noise spectroscopy with scanning tunneling microscopy (STM) has proven to be a powerful technique to investigate the electronic properties of quantum materials. It provides direct and non-invasive insight into the tunneling charge quanta or dynamics at the atomic scale. Due to the typically weak noise signal and the presence of low frequency spurious noise, local noise experiments require a high-resolution measurement amplifier. Here, we present a newly developed high-resolution noise amplifier that we implemented in three different STMs. Compared to our previous generation, we obtain more than a 20-fold improvement in the noise resolution, allowing us to resolve values of the effective charge as small as 0.01*e*. Our amplifier opens new possibilities for studying electronic properties in novel materials such as d-wave superconductors. In addition to this, it can give direct information about the local electron temperature in STM experiments.

I. INTRODUCTION

Quantum materials often exhibit a plethora of exotic behaviors. Notable examples include the emergence of superconductivity, where resistance vanishes below a material-dependent critical temperature (T_c), and the fractional quantum Hall effect, characterized by the quantization of Hall conductance to fractional values of the quantum of conductance in two-dimensional electron systems.

One of the methods to experimentally probe the electronic properties of quantum materials is noise spectroscopy. Shot noise arises from the discrete nature of electric charge carriers and their probabilistic transport across potential barriers, leading to fluctuations in the current.[1] This noise can contain information about electronic correlations and dynamical phenomena. Shot noise has been used to directly detect, for example, the effective charge in Andreev reflections,[2–4] the fractional charge of the quasiparticles in the fractional quantum Hall effect (FHQE),[5,6] and Coulomb interactions in quantum dots.[7,8] In addition to this, it can also give information about the fundamental noise floor in nonlinear superconducting readout/detector circuits.[9] In a tunnel junction, shot noise can give information about the correlations in the tunneling events. In the limit of low transparencies, the zero-temperature power spectral density of current shot noise in a tunnel junction is given by[1] $S = 2qI$, where q is the effective charge of the carriers and I is the time-averaged value of the current. The effective charge encodes information about the statistical distribution of the tunneling events in time. Uncorrelated processes would lead to $q = 1e$, whereas in the presence of strong electronic correlations $q \neq 1e$.

Including thermal effects, the power spectral density of shot noise through the junction takes the following form:[10]

$$S = 2qI \coth\left(\frac{qV}{2k_BT}\right), \quad (1)$$

where V is the voltage applied across the junction, k_B is the Boltzmann constant, and T is the temperature. When $qV \ll 2k_BT$, we obtain the thermal contribution to the junction noise $S = \frac{4k_BT}{R}$. It is important to note, however, that not all forms of relevant noise are captured by Eq. (1); examples include super-Poissonian noise,[11,12] telegraph noise,[13–15] and other fluctuations that can dominate the junction noise and provide information about the electronic properties of the materials.[16]

Recently, shot noise readout was combined with scanning tunneling microscopy (STM) to realize noise-STM.[17–20] Noise-STM allows shot noise measurements on the atomic scale, which can offer a deeper understanding of how spatial inhomogeneities,[21] local defects, and impurities[11,12,22] can influence the electronic states, and yields information on pairing.[4,21,23,24] Moreover, the STM often operates in the limit of a single transmission channel with tunable junction transparency, providing information on superconductors more reliably than mesoscopic devices, which feature multiple parallel channels.[25] However, noise-STM requires an extremely high-resolution amplifier due to the small shot noise signal of the junction (typically, currents of less than 1 nA are used, which corresponds to a noise power of ~320 fA^2/Hz) compared to the large low frequency mechanical and $1/f$ noises in the STM.[26] Here, we present a high-resolution cryogenic amplifier for noise-STM, which shows a 20-fold resolution improvement with respect to our previous study.[17] This allows us to measure variations in the effective charge as small as $0.01e$, which is of special relevance to capture correlation effects in systems where both correlated and uncorrelated electrons contribute to the tunnel current, such as in d-wave superconductors.

II. OVERALL DESIGN OF THE CRYOGENIC AMPLIFIER

We begin by describing the basic design of our cryogenic amplifier. Its development requires special considerations, as noise-STM presents different challenges compared to conventional mesoscopic devices. In particular, the junction resistance in STM is much higher (MΩ – GΩ) than the typical values of mesoscopic devices (Ω – kΩ). This junction resistance, together with the wire capacitance, will form a low pass filter with a bandwidth from DC to a few kilohertz, where mechanical and $1/f$ noises are dominant. To circumvent this, we designed a new, ultra-sensitive amplifier based

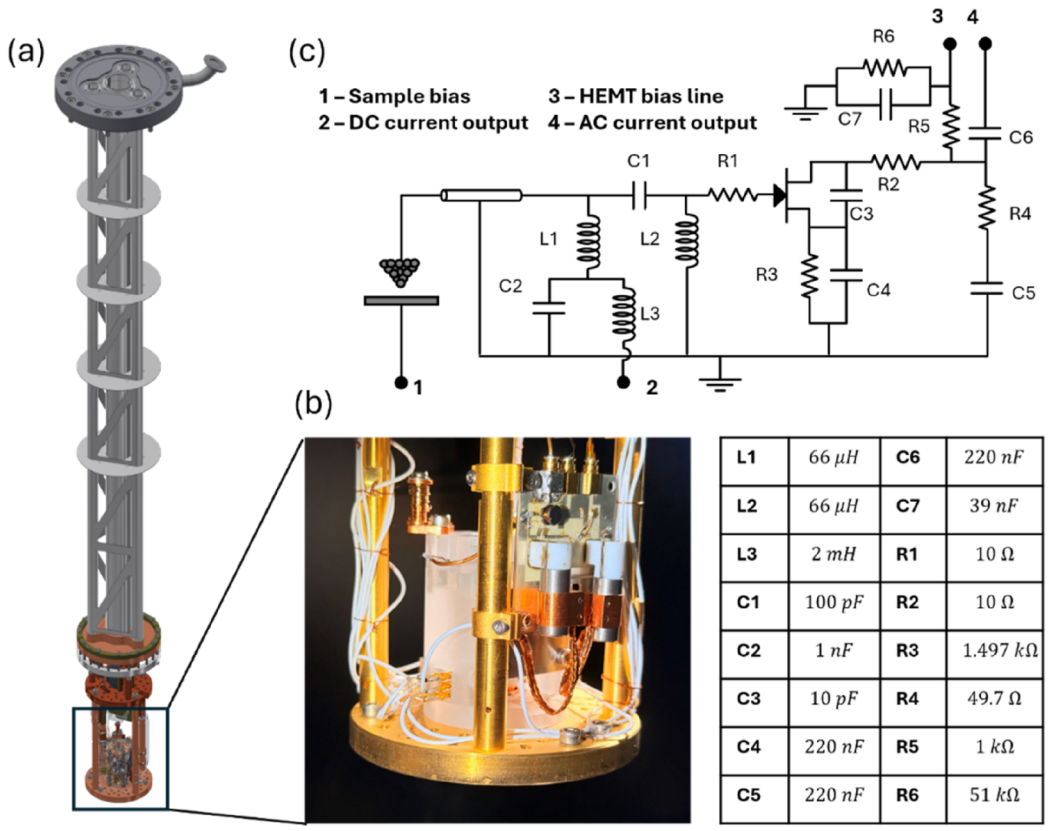

L1	66 μH	C6	220 nF
L2	66 μH	C7	39 nF
L3	2 mH	R1	10 Ω
C1	100 pF	R2	10 Ω
C2	1 nF	R3	1.497 $k\Omega$
C3	10 pF	R4	49.7 Ω
C4	220 nF	R5	1 $k\Omega$
C5	220 nF	R6	51 $k\Omega$

FIG. 1. Design of the newly developed high-resolution cryogenic noise amplifier. (a) Top-loading insert of the custom-built 4.2 K STM system. (b) Photograph of the STM head and integrated cryogenic low-noise amplifier. (c) Schematic diagram of the amplifier circuit shown in (b); component values are listed in the accompanying table.

on our earlier design and implemented it in three STMs [an ultra-stable home-built STM at 4.2 K,[27] a UNISOKU Ltd USM1300 with a base temperature of 340 mK and equipped with a vector magnetic field (2/2/9 T), and a UNISOKU USM1500 with a base temperature of 2.2 K and a magnetic field of 8 T]. Below, we focus on the implementation in the home-built setup unless noted otherwise.

Figure 1 shows an overview of the insert of our home-built setup, with the STM head and cryogenic amplifier located at the bottom [see Fig. 1(b)]. The circuit, including the STM junction, cryogenic amplifier, and the wiring to room temperature, is shown in Fig. 1(c). The amplifier contains two LC resonator tanks (L1 and L2) with a resonance frequency of 4.2 MHz and a high electron-mobility transistor (HEMT).[28,29] Each LC resonator is formed by the inductance of a superconducting niobium (Nb) coil and its corresponding parasitic capacitance. The Nb wire is laser-welded to a Cu wire, which is then soldered to the printed circuit board (PCB). The PCB is mechanically mounted to a gold-plated, oxygen-free copper frame, which is thermally anchored to the liquid helium bath of the cryostat.

The DC current goes directly to the conventional STM feedback system, allowing simultaneous high-frequency noise measurements and regular STM operation. The current noise at the resonance frequency is amplified and converted into voltage noise by the cryogenic HEMT amplifier (CryoHEMT, model 5pch[30]), which has been extensively characterized in the literature.[29,31,32] In the circuit, R1, R2, and C3 are used to improve the stability of the amplifier circuit. R3 is the source resistor, R5 is the drain resistor, and R4 is the output impedance of the amplifier. R6 combined with C7 is a low temperature low pass filter to improve the stability of the HEMT working bias. We note here that our amplifier does not amplify the voltage of the signal, but—because the output is 50 Ω while the input is high ohmic (MΩ–GΩ)—it does amplify the power. Next, our noise signal is amplified by a commercial room temperature amplifier (FEMTO HAS-X-1-40) and recorded by a spectrum analyzer (Zurich Instruments HF2LI or MFLI). From the measured voltage noise (S_V^m) at the spectrum analyzer, we obtain the current noise (S_I) at the junction by inverting the following equation:

$$S_V^m = G^2 * \left|Z_{tot}^2\right| * S_I^{tot} + BG_0^V, \tag{2}$$

where G is the total effective gain of the amplifier chain, $Z_{tot} = Z_{LC} // R_j^{diff}$ is the total impedance of the LC resonators Z_{LC}, and the differential junction resistance of the STM R_j^{diff}. The total current noise $S_I^{tot} = S_I + BG_1^I$ includes both the shot noise from the STM junction (S_I) and the effective background current noise from the amplifier (BG_1^I). BG_0^V is the effective background voltage noise of the amplifier chain and spectrum analyzer.

III. BASIC AMPLIFIER PROPERTIES: Q FACTOR, RESONANCE FREQUENCY, SATURATION CURVE, AND CIRCUIT IMPEDANCE

In this section, we will present the basic information about our amplifier. The HEMT saturation curve and circuit resonances measured at two different temperatures are shown in Fig. 2. The blue and red lines in Fig. 2(a) correspond to the saturation curves {I_{sd} vs V_{HEMT}, where I_{sd} is the source–drain current of the HEMT and V_{HEMT} is the voltage applied to the amplifier bias input [port 3 in Fig. 1(c)]} at 4.2 and 77 K, respectively. The saturation curves indicate the bias at which we find the optimal working point of the HEMT.

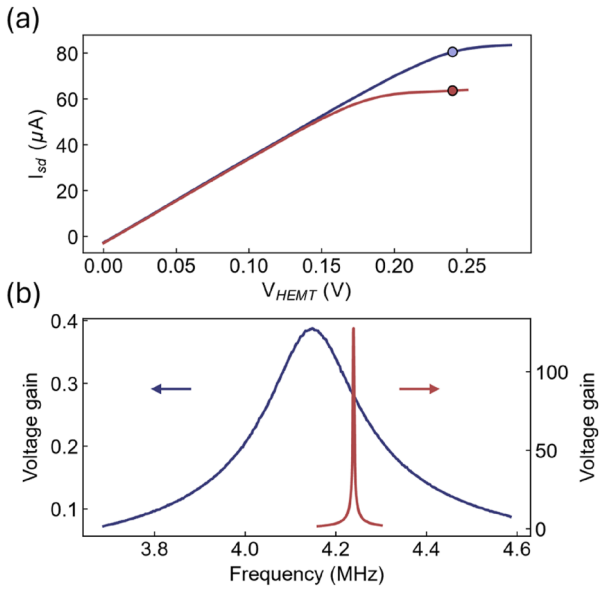

FIG. 2. (a) Current–voltage (I–V) characteristics of the HEMT measured at 77 K (blue curve) and 4.2 K (red curve). (b) Frequency-dependent voltage gain of the cryogenic amplifier at 77 K (blue curve) and 4.2 K (red curve), corresponding to the V_{HEMT} = 235 mV indicated by the blue and red markers in (a).

The measured frequency response of the voltage gain for each of these temperatures at a HEMT bias of 235 mV [indicated by the blue and red markers in Fig. 2(a)] is shown in Fig. 2(b). The blue curve is measured at 77 K, with an input root-mean-square voltage amplitude (V_{RMS}) of 400 μV applied to the STM bias [port 1 in Fig. 1(c)] through a frequency sweeping AC voltage generator of Zurich Instruments HF2LI. The red curve is obtained at 4.2 K, below T_c of the Nb coils (T_c ~ 9 K), and input V_{RMS} = 30 μV. The quality factor (Q-factor) increases significantly when the temperature cools below T_c, which increases the signal amplitude and the resolution of our amplifier.

The HEMT power dissipation is minimal: with an operating voltage of 235 mV and a current of 63.6 μA, the total power consumption is P = 14.9 μW. This very low dissipation ensures that the cryostat temperature remains stable during all measurements.

To achieve our goals, we have implemented several design changes. The homemade superconducting inductors are made by cross-winding niobium wire (diameter 0.1 mm) around a custom-designed glass-ceramic (Macor) frame, and each of them has an individual Nb shield around it to prevent eddy current dampening, as shown in Fig. 1(b). The amplifier is designed in such a way that the distance to the STM is minimized, reducing the length of the wire (8 cm) connecting the tip and amplifier, and hence, its capacitance (29.5 pF/ft). This allows us to obtain a higher resonance frequency with a higher Q-factor of the overall circuit, shifting the working point of the amplifier further away from the $1/f$ noise contribution and, therefore, improving the signal-to-noise ratio. As a result,

the Q-factor of our amplifier reaches ~2000 at 4.2 MHz, significantly exceeding the reported value of ~700 at 3 MHz[17] and ~25 at 1 MHz.[18] In addition, the circuit contains several low pass filters (details below), as shown in Fig. 1(c), to decouple the cryogenic amplifier from spurious room temperature noises like thermal noise. The output impedance of the cryogenic amplifier (50 Ω) is designed to match that of the cabling leading to the room temperature amplifier. CuNi-based semirigid coaxial cables and high-frequency SMA connectors are used to connect the cryogenic part of the circuit to the room temperature amplifier.

Figure 3(a) shows the broad bandwidth spectral density of the noise signal measured with the STM tip retracted (I_{DC} = 0 nA, I_{DC} being the current through the STM tunnel junction, applied via port 1—sample bias). The spectral features at frequencies below 1 MHz and above 5 MHz are due to the room-temperature bandpass filters (Mini-Circuits ZFHP-1R2-S+ and BLP-5+), which shape the PSD based on the reflection principle. The two resonances observed at 1.5 and 4.2 MHz are generated by the double tank circuit. The relative amplitude of the two resonances is mainly determined by the coupling capacitor C_1. For precise noise measurements, the resonance with a higher frequency is used, as $1/f$ noise is more prominent at lower frequencies. A demodulator at f = 4.2 MHz is applied, enabling us to measure more spectral data points centered around the resonance, which also improves the noise resolution, as shown in Fig. 3(b). More information about how the demodulator downconverts and processes the signal can be found in Ref. 33. The power spectral density (PSD) is measured with a bandwidth of 400 kHz and consists of 65 536 frequency points. The data are averaged over 5 min, with a total of 2000 spectra. To extract the noise power S_I, this spectrum is fitted with Eq. (2). The resulting fit line is shown as a black dashed line in Fig. 3(b). G and BG_1^I are calibrated on an Au(111) surface by measuring shot noise at different biases.

Figure 3(c) shows the time evolution of S_I for 1, 1.25, and 1.5 mV bias voltages with a fixed junction resistance R_j = 12.5 MΩ. Each of the data points is the outcome of fitting the resonance that has been averaged for 5 min. The state-of-the-art stability of the measurements can be observed from the fluctuations around the time averaged value of S_I, which have a spread of only ~3 fA^2/Hz. To enhance the stability of the amplifier, low-pass filters were added to both the amplifier bias and STM bias lines to suppress external electrical noise, as we discussed earlier. In addition, the amplifier operates at low power and is well thermalized to the cold bath, with a stabilized dewar pressure to prevent temperature fluctuations over time. The resolution of S_I is estimated from the standard deviation of these points, σ, which varies with averaged time [Fig. 3(d)]. At an averaging time of ~10 min, the standard deviation of our current amplifier is ~0.5 fA^2/Hz, about 20 times smaller than the ~10 fA^2/Hz estimated from our previous study[17] under similar measurement conditions. We can also estimate the uncertainty in the extracted value of the effective charge at a given current by $\sigma/2eI$.

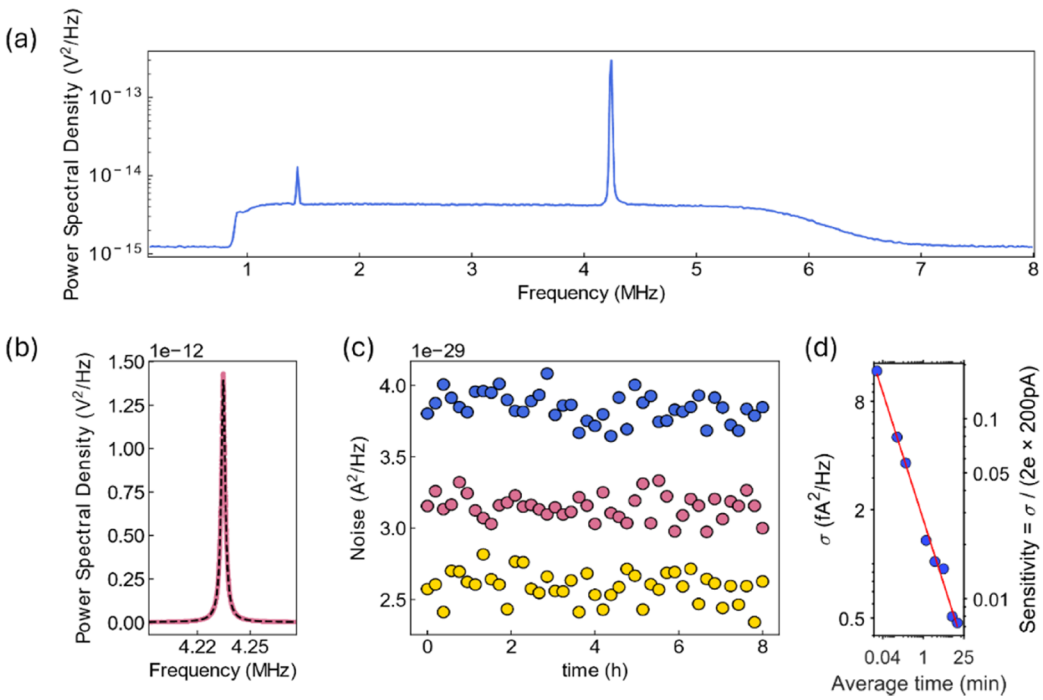

FIG. 3. (a) Large-bandwidth power spectral density of the measured signal with the cryogenic noise amplifier at 4.2 K and V_{HEMT} = 235 mV. (b) Power spectral density measurement (pink curve) and fitting model (black dashed line) of a small bandwidth around the highest resonance frequency at 4.23 MHz. (c) Current-noise measurements as a function of time. Each point is obtained from fitting the power spectral density curve with Eq. (2) at a STM bias voltage of 1 mV (yellow points), 1.25 mV (pink points), and 1.5 mV (blue points) for a measure and for an averaging time of 5 min. (d) Standard deviation and estimated sensitivity of the current noise fluctuations in time for different averaging times. The sensitivity indicates the effective charge resolution and is estimated from the shot noise formula $S = 2qI$, for a typical current of 200 pA.

For a typical tunneling current of 200 pA, the corresponding effective charge resolution is shown on the right y axis of Fig. 3(d). It decreases below 0.01e for averaging times longer than 5 min.

IV. HIGH-RESOLUTION SHOT NOISE SPECTROSCOPY ON A METAL AND A SUPERCONDUCTOR

Figure 4(a) shows noise measurements as a function of tunneling current on an Au(111) surface, as well as the resolved effective charge [Fig. 4(b)]. During the measurement, the STM junction resistance is constant (R_j = 1 GΩ), and the feedback is enabled to achieve optimal junction stability. The data were collected with both the previous amplifier (yellow dots)[17] at 2.3 K and our present amplifier (blue dots) at 4 K, with all other measurement parameters, such as averaging time (~10 min), kept the same. The increased sensitivity to shot noise allows us to resolve much smaller deviations in the effective charge.

When tunneling into a superconductor, Andreev reflections contribute to the noise signal by effectively transferring charge in units of 2e, thereby doubling the noise compared to single-electron tunneling processes.[4] Figures 4(c) and 4(d) display the measured noise and the corresponding effective charge, respectively, as a function of bias voltage for a niobium diselenide ($NbSe_2$) sample. The data are obtained at 340 mK using a UNISOKU Ltd. USM1300 system, with a metallic tip and a constant DC junction resistance of 1.5 MΩ. A clear enhancement in noise due to Andreev processes is observed at low bias voltages, below the superconducting gap (Δ = 1.0 meV), where the effective charge smoothly transitions toward 2e. This represents a significant improvement over previous studies, since a 2e effective charge in noise STM has only been reported using superconducting tips.[4,22,23,25]

Beyond the conventional superconductors, the improved resolution demonstrated here opens the possibility for investigating systems in which correlated electron processes contribute only a small fraction of the total tunneling events, such as in cuprate high-temperature superconductors,[21] where both 1e and 2e processes coexist, and the resulting enhancement of the effective charge can be as small as a few percent of the electron charge.

V. PERFORMANCE UNDER MAGNETIC FIELD

The performance of the shot noise amplifier was evaluated in a UNISOKU Ltd. USM1300 system under varying magnetic field strengths to assess its stability and reliability. Figure 5(a) shows the Q-factor of the resonance, extracted from PSD measurements, as a function of magnetic field in the Z-axis (perpendicular to the sample). We performed these measurements at 1.8 K with the tip retracted, using 2000 averages per point (~5 min per measurement).

To facilitate experiments in strong magnetic fields, the amplifier is positioned ~20 cm above the center of the magnetic field. At the amplifier's location, the magnetic field strength is much lower than at the sample site, enabling high-field measurements while minimizing the impact of the field on amplifier performance. This design ensures that the amplifier remains stable and maintains high resolution even under strong magnetic fields. As the magnetic field increases, the Q-factor gradually decreases, likely due to eddy current damping induced by the external magnetic field. The inset displays PSD curves as a function of frequency, each taken at a

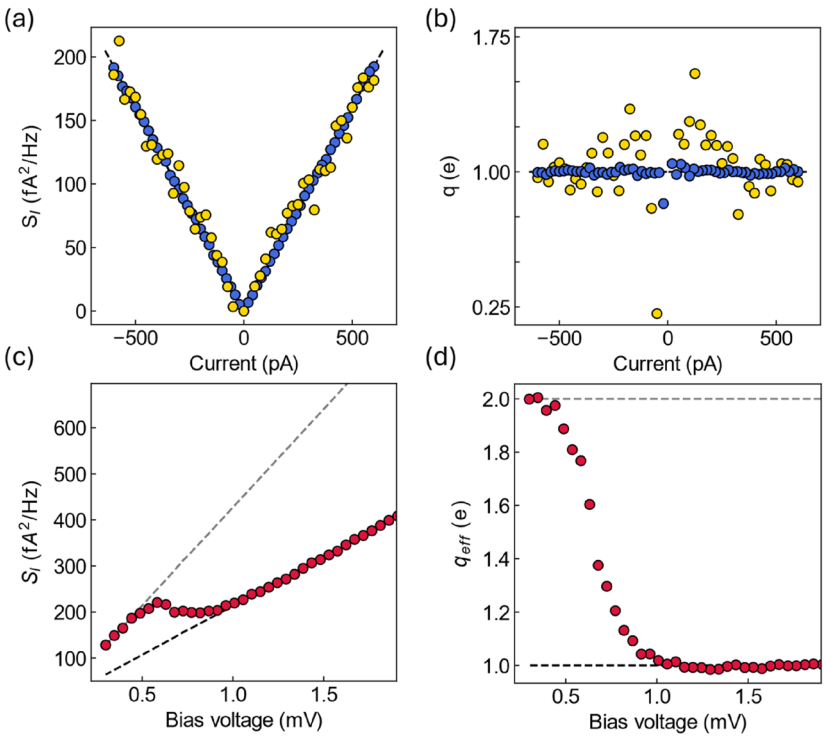

FIG. 4. Single-position noise spectra and corresponding effective charge as a function of tunneling current or bias voltage (interchangeable under fixed junction resistance conditions) for (a) and (b) gold on mica (measured at T = 4.2 K) and (c) and (d) superconducting $NbSe_2$ (measured at 300 mK) samples. In (a) and (b), yellow data points represent measurements taken with the previous-generation amplifier, reproduced from Bastiaans *et al.*, Rev. Sci. Instrum. **89**, 093709 (2018) with the permission of AIP Publishing LLC.[17] The blue points correspond to measurements using the newly implemented amplifier.

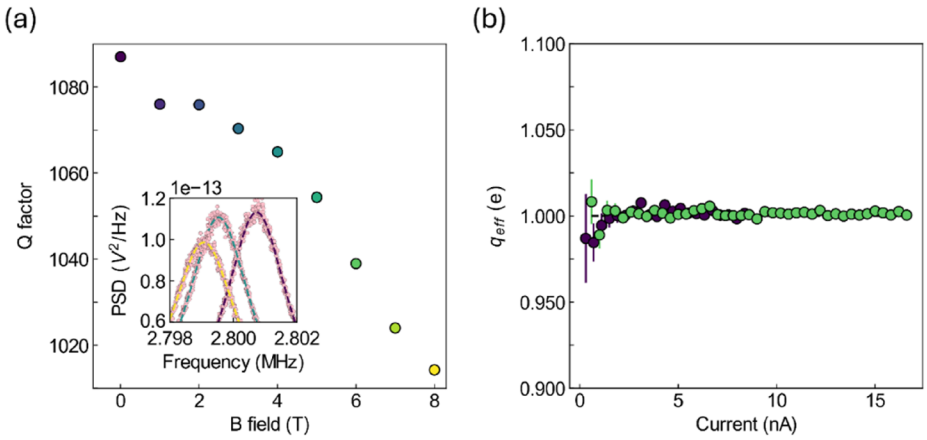

FIG. 5. Magnetic field-dependent noise measurements. (a) Quality factor of the resonance extracted from fits to the noise power spectral density at magnetic field strengths from 0 to 8 T. Example fits for 0, 4, and 8 T are shown in the inset. (b) Effective charge as a function of tunneling current measured on a gold-on-mica sample at magnetic fields of 0 T (dark purple) and 6 T (green).

different magnetic field strength. These curves show a shift in resonance frequency with increasing field, while the overall resonance remains well-defined.

Importantly, the magnetic field has only a minor effect on the Q-factor and negligible impact on the amplifier's effective charge resolution. This is further demonstrated in Fig. 5(b), which presents the effective charge obtained from noise measurements on an Au(111) as a function of tunneling current at 0 T (dark purple) and 6 T (green). The effective charge resolution remains similar for both measurements, confirming that the amplifier maintains its performance in magnetic fields up to at least 6 T.

VI. LOCAL ELECTRON TEMPERATURE THERMOMETER

Our shot noise STM also offers an additional novel application as an atomic scale electron-temperature thermometer. The electron temperature of the STM junction is difficult to measure, and it may not be identical to the base temperature of the system because of combinations of local Joule heating, limited filtering, and poor electron–phonon temperature equilibration. Often, the system's electron temperature is extracted from a model-dependent fitting of the STS spectra of a superconducting sample and/or with a superconducting tip.[34] However, this method is imprecise, as it depends on the specific model used for fitting.[35–37] Furthermore, this method cannot be used for non-superconducting but still important classes of materials such as metals, semiconductors, and topological insulators. Our shot noise STM offers a generally applicable way to measure the electron temperature directly.[18,19] At sufficiently low bias voltages, the coth factor in Eq. (1) is no longer ignored, and the shot noise signal is sensitive to the electron temperature T_e. Measuring shot noise S_I at low bias ($eV < k_B T_e$) can therefore be used to accurately measure T_e. Figure 6 shows the shot noise measured at a bias range from 3 to −3 mV for two different temperatures on Au(111) with R_j = 5 MΩ. The blue dots are measured in our home-built STM with T_{base} ~ 4.2 K, and the red dots are measured in UNISOKU USM1500 with T_{base} ~ 2.2 K. As expected, when $eIR_j \sim 2k_B T_e$, shot noise will show non-linear behavior with current I. By fitting the curves, we extract T_e = 4.35 K and T_e = 2.51 K, respectively. These results demonstrate that our ultra-sensitive shot noise STM provides a more accurate and broadly applicable method

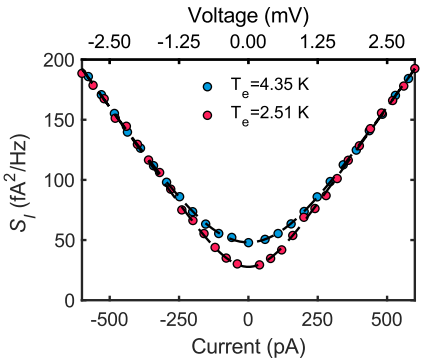

FIG. 6. Noise spectra as a function of tunneling current (for a bias range from −3 to 3 mV and a junction resistance of 5 MΩ) measured at different temperatures. Electron temperatures extracted by fitting the data (black dashed lines) using Eq. (2) are indicated in the legend.

to measure the electron temperature at the atomic scale, even in systems where traditional spectroscopic approaches fail.

VII. CONCLUSIONS

We have developed an improved cryogenic amplifier for STM based noise measurements and integrated it into three setups. Our setups allow for the detection of effective charge variations as small as 0.01e, enabling precise measurements of electron correlations in novel quantum materials. This advancement opens new possibilities for exploring correlated electron systems, including cuprate high-temperature superconductors, where both 1e and 2e tunneling processes coexist. Beyond noise spectroscopy, our system also provides a novel method for measuring the electron temperature on the atomic scale. Our technique enables accurate electron temperature detection on a wide range of metallic surfaces, offering broader applicability in nanoscale studies.

ACKNOWLEDGMENTS

This study was supported by the European Research Council (ERC StG SpinMelt and ERC CoG PairNoise). I.S., M.O.L., and

J.P.C. were supported by the European Research Council (Horizon 2020 "FRACTAL," No. 865570). I.S. acknowledges the Gravitation research program "Materials for the Quantum Age" (QuMat) (Registration No. 024.005.006), financed by the Dutch Ministry of Education, Culture and Science (OCW). A.M. acknowledges the Netherlands Organisation for Scientific Research (NWO/OCW), as part of the Frontiers of Nanoscience program (No. NF21CAS18).

AUTHOR DECLARATIONS

Conflict of Interest

The authors have no conflicts to disclose.

Author Contributions

Maialen Ortego Larrazabal and Jiasen Niu contributed equally to this study.

Maialen Ortego Larrazabal: Data curation (equal); Formal analysis (equal); Investigation (equal); Methodology (equal); Software (equal); Validation (equal); Visualization (equal); Writing – original draft (equal); Writing – review & editing (equal). **Jiasen Niu**: Data curation (equal); Formal analysis (equal); Investigation (equal); Methodology (equal); Software (equal); Validation (equal); Visualization (equal); Writing – original draft (equal); Writing review – editing (equal). **Jian-Feng Ge**: Investigation (supporting); Methodology (supporting); Software (equal); Writing – review & editing (supporting). **Yudai Sato**: Data curation (supporting); Investigation (supporting); Methodology (supporting); Software (supporting); Writing – review & editing (supporting). **Jan P. Cuperus**: Data curation (supporting); Investigation (supporting); Methodology (supporting); Software (supporting); Writing – review & editing (supporting). **Tjerk Benschop**: Investigation (supporting); Methodology (supporting); Software (supporting); Writing – review & editing (supporting). **Koen M. Bastiaans**: Investigation (supporting); Methodology (supporting); Software (supporting); Writing – review & editing (supporting). **Amber Mozes**: Investigation (supporting); Methodology (supporting); Software (supporting); Writing – review & editing (supporting). **Ingmar Swart**: Conceptualization (equal); Funding acquisition (equal); Investigation (equal); Project administration (equal); Resources (equal); Supervision (equal); Validation (equal); Writing – review & editing (equal). **Milan P. Allan**: Conceptualization (equal); Funding acquisition (equal); Investigation (equal); Project Administration (equal); Resources (equal); Supervision (equal); Validation (equal); Writing – review & editing (equal).

DATA AVAILABILITY

All data used to generate the figures are available on Zenodo at https://doi.org/10.5281/zenodo.16985850.

REFERENCES

[1]Ya. M. Blanter and M. Büttiker, "Shot noise in mesoscopic conductors," Phys. Rep. **336**, 1 (2000).
[2]X. Jehl, P. Payet-Burin, C. Baraduc, R. Calemczuk, and M. Sanquer, "Andreev reflection enhanced shot noise in mesoscopic SNS junctions," Phys. Rev. Lett. **83**, 1660 (1999).
[3]Y. Ronen, Y. Cohen, J.-H. Kang, A. Haim, M.-T. Rieder, M. Heiblum, D. Mahalu, and H. Shtrikman, "Charge of a quasiparticle in a superconductor," Proc. Natl. Acad. Sci. **113**, 1743 (2016).
[4]K. M. Bastiaans, D. Cho, D. Chatzopoulos, M. Leeuwenhoek, C. Koks, and M. P. Allan, "Imaging doubled shot noise in a Josephson scanning tunneling microscope," Phys. Rev. B **100**, 104506 (2019).
[5]R. de-Picciotto, M. Reznikov, M. Heiblum, V. Umansky, G. Bunin, and D. Mahalu, "Direct observation of a fractional charge," Nature **389**, 162 (1997).
[6]L. Saminadayar, D. C. Glattli, Y. Jin, and B. Etienne, "Observation of the e/3 fractionally charged laughlin quasiparticle," Phys. Rev. Lett. **79**, 2526 (1997).
[7]E. Onac, F. Balestro, B. Trauzettel, C. F. J. Lodewijk, and L. P. Kouwenhoven, "Shot-noise detection in a carbon nanotube quantum dot," Phys. Rev. Lett. **96**, 026803 (2006).
[8]A. Thielmann, M. H. Hettler, J. König, and G. Schön, "Cotunneling current and shot noise in quantum dots," Phys. Rev. Lett. **95**, 146806 (2005).
[9]R. N. Jabdaraghi, D. S. Golubev, J. P. Pekola, and J. T. Peltonen, "Noise of a superconducting magnetic flux sensor based on a proximity Josephson junction," Sci. Rep. **7**, 8011 (2017).
[10]D. Rogovin and D. J. Scalapino, "Fluctuation phenomena in tunnel junctions," Ann. Phys. **86**, 1 (1974).
[11]K. M. Bastiaans, D. Cho, T. Benschop, I. Battisti, Y. Huang, M. S. Golden, Q. Dong, Y. Jin, J. Zaanen, and M. P. Allan, "Charge trapping and super-Poissonian noise centres in a cuprate superconductor," Nat. Phys. **14**, 1183 (2018).
[12]F. Massee, Y. K. Huang, M. S. Golden, and M. Aprili, "Noisy defects in the high-T_c superconductor $Bi_2Sr_2CaCu_2O_{8+x}$," Nat. Commun. **10**, 544 (2019).
[13]L. Desvignes, V. S. Stolyarov, M. Aprili, and F. Massee, "Tunable high speed atomic rotor in Bi_2Se_3 revealed by current noise," ACS Nano **15**, 1421 (2021).
[14]T. Werkmeister, J. R. Ehrets, M. E. Wesson, D. H. Najafabadi, K. Watanabe, T. Taniguchi, B. I. Halperin, A. Yacoby, and P. Kim, "Anyon braiding and telegraph noise in a graphene interferometer," Science **388**, 730–735 (2025).
[15]B. Kiraly, E. J. Knol, W. M. J. van Weerdenburg, H. J. Kappen, and A. A. Khajetoorians, "An atomic Boltzmann machine capable of self-adaption," Nat. Nanotechnol. **16**, 414 (2021).
[16]J. Sun, J. Niu, Y. Li, Y. Liu, L. N. Pfeiffer, K. W. West, P. Wang, and X. Lin, "Dynamic ordering transitions in charged solid," Fundam. Res. **2**, 178 (2022).
[17]K. M. Bastiaans, T. Benschop, D. Chatzopoulos, D. Cho, Q. Dong, Y. Jin, and M. P. Allan, "Amplifier for scanning tunneling microscopy at MHz frequencies," Rev. Sci. Instrum. **89**, 093709 (2018).
[18]F. Massee, Q. Dong, A. Cavanna, Y. Jin, and M. Aprili, "Atomic scale shot-noise using cryogenic MHz circuitry," Rev. Sci. Instrum. **89**, 093708 (2018).
[19]U. Kemiktarak, T. Ndukum, K. C. Schwab, and K. L. Ekinci, "Radio-frequency scanning tunnelling microscopy," Nature **450**, 85 (2007).
[20]I. Tamir, V. Caspari, D. Rolf, C. Lotze, and K. J. Franke, "Shot-noise measurements of single-atom junctions using a scanning tunneling microscope," Rev. Sci. Instrum. **93**, 023702 (2022).
[21]J. Niu, M. Ortego Larrazabal, T. Gozlinski, Y. Sato, K. M. Bastiaans, T. Benschop, J.-F. Ge, Y. M. Blanter, G. Gu, I. Swart, and M. P. Allan, "Equivalence of pseudogap and pairing energy in a cuprate high-temperature superconductor," arXiv:2409.15928.
[22]U. Thupakula, V. Perrin, A. Palacio-Morales, L. Cario, M. Aprili, P. Simon, and F. Massee, "Coherent and incoherent tunneling into Yu-Shiba-Rusinov states revealed by atomic scale shot-noise spectroscopy," Phys. Rev. Lett. **128**, 247001 (2022).
[23]J.-F. Ge, K. M. Bastiaans, J. Niu, T. Benschop, M. Ortego Larrazabal, and M. P. Allan, "Direct visualization of quasiparticle concentration around superconducting vortices," Appl. Phys. Lett. **125**, 252601 (2024).
[24]K. M. Bastiaans, D. Chatzopoulos, J.-F. Ge, D. Cho, W. O. Tromp, J. M. van Ruitenbeek, M. H. Fischer, P. J. de Visser, D. J. Thoen, E. F. C. Driessen *et al.*, "Direct evidence for Cooper pairing without a spectral gap in a disordered superconductor above T_c," Science **374**, 608 (2021).
[25]J. Niu, K. M. Bastiaans, J.-F. Ge, R. Tomar, J. Jesudasan, P. Raychaudhuri, M. Karrer, R. Kleiner, D. Koelle, A. Barbier, E. F. C. Driessen, Y. M.

Blanter, and M. P. Allan, "Why shot noise does not generally detect pairing in mesoscopic superconducting tunnel junctions," Phys. Rev. Lett. **132**, 076001 (2024).
[26]S. Sugita, Y. Mera, and K. Maeda, "Origin of low frequency noise and 1/f fluctuations of tunneling current in scanning tunneling microscopes," J. Appl. Phys. **79**, 4166 (1996).
[27]I. Battisti, G. Verdoes, K. van Oosten, K. M. Bastiaans, and M. P. Allan, "Definition of design guidelines, construction, and performance of an ultra-stable scanning tunneling microscope for spectroscopic imaging," Rev. Sci. Instrum. **89**, 123705 (2018).
[28]Y. Jin, Q. Dong, U. Gennser, L. Couraud, A. Cavanna, and C. Ulysse, "Ultra-low noise CryoHEMTs for cryogenic high-impedance readout electronics: Results and applications," in *2016 13th IEEE International Conference on Solid-State and Integrated Circuit Technology (ICSICT)* (IEEE, 2016), pp. 342–345.
[29]Q. Dong, Y. X. Liang, D. Ferry, A. Cavanna, U. Gennser, L. Couraud, and Y. Jin, "Ultra-low noise high electron mobility transistors for high-impedance and low-frequency deep cryogenic readout electronics," Appl. Phys. Lett. **105**, 013504 (2014).
[30]CryoHEMT—Electronics for scientific research, https://cryohemt.com/
[31]G. Baulieu, J. Billard, G. Bres, J.-L. Bret, D. Chaize, J. Colas, Q. Dong, O. Exshaw, C. Guerin, S. Ferriol *et al.*, "HEMT-based 1 K front-end electronics for the heat and ionization Ge CryoCube of the future ricochet CEvNS Experiment," J. Low Temp. Phys. **209**, 570 (2022).
[32]Y. Jin, Q. Dong, Y. X. Liang, A. Cavanna, U. Gennser, L. Couraud, and C. Ulysse, "Ultra-low noise HEMTs for high-impedance and low- frequency preamplifiers: realization and characterization from 4.2 K to 77 K," J. Phys.: Conf. Ser. **568**, 032009 (2014).
[33]MFLI 500 kHz/5 MHz Lock-in Amplifier|Zurich Instruments, https://www.zhinst.com/europe/en/products/mfli-lock-in-amplifier
[34]T. Esat, X. Yang, F. Mustafayev, H. Soltner, F. S. Tautz, and R. Temirov, "Determining the temperature of a millikelvin scanning tunnelling microscope junction," Commun. Phys. **6**, 81 (2023).
[35]M. Ruby, B. W. Heinrich, J. I. Pascual, and K. J. Franke, "Experimental demonstration of a two-band superconducting state for lead using scanning tunneling spectroscopy," Phys. Rev. Lett. **114**, 157001 (2015).
[36]M. Uhl, P. Kot, R. Drost, H. Huang, J. Ankerhold, J. C. Cuevas, and C. R. Ast, "Multiband Josephson effect in an atomic scale Pb tunnel junction," Phys. Rev. Res. **6**, 043233 (2024).
[37]Y. Noat, J. A. Silva-Guillén, T. Cren, V. Cherkez, C. Brun, S. Pons, F. Debontridder, D. Roditchev, W. Sacks, L. Cario, P. Ordejón, A. García, and E. Canadell, "Quasiparticle spectra of 2H-$NbSe_2$: Two-band superconductivity and the role of tunneling selectivity," Phys. Rev. B **92**, 134510 (2015).